JOURNAL OF SPACECRAFT AND ROCKETS
Vol. 45, No. 1, January–February 2008

Improvement of High Heat Flux Measurement Using a Null-Point Calorimeter

Stefan Löhle* and Jean-Luc Battaglia†
Université de Bordeaux I, 33405 Talence, France
Pierre Jullien‡ and Bruno van Ootegem‡
European Aeronautic Defense and Space Company, 33165 Saint-Médard en Jalles, France
and
Jacques Couzi§ and Jean-Pierre Lasserre§
Commissariat à l'Energie Atomique/Centre d'Études Scientifiques et Techniques d'Aquitaine, 33114 Le Barp, France

DOI: 10.2514/1.30092

A novel approach to analyze null-point calorimeter data in high enthalpy and high pressure plasma flows is described. Although null-point calorimetry is a well-known measurement technique, the measurements of recent campaigns showed unphysical effects. Usually, radial heat flux profiles, i.e., heat flux profiles perpendicular to the flow axis, are recorded. These profiles show asymmetries, although the generator's setup is symmetric. Within this paper, the reasons for this asymmetry are shown by a theoretical approach using finite element modeling. One major concern is that because of the short measurement times, the thermocouple inertia becomes crucial. In the present case, surface heat flux is therefore determined by solving the inverse heat conduction problem using a noninteger identified model as a direct model for the estimation process. The sensor calibration is performed using high-power laser radiation. With the new calibration data, the asymmetries vanish and it is discussed that the measured heat flux profiles can be reasonably interpreted with the present methodology according to turbulent freejet theory.

Nomenclature

c_p	=	specific heat, J/(kg · K)
D	=	differentiation operator, m
E	=	energy, J
f	=	function
T	=	temperature, K
t	=	time, s
V_T	=	thermocouple signal, V
x	=	distance, m
α, β	=	model parameters, V
ϵ	=	emissivity
λ	=	thermal conductivity, W/(m · K)
ρ	=	density, kg/m^3
ϕ	=	heat flux, W/m^2

I. Introduction

KENNEDY et al. first proposed transient heat flux measurements using swept null-point calorimetry in 1972 [1]. They published a copper sensor design, the form of which is still in use. It is shown in Fig. 1. The interior design of the sensor is shown in Fig. 2. The heat flux is estimated from a temperature measurement. The location of the temperature measurement is chosen such that the null-point scenario is given [2,3]. This means that the measured temperature history at the backside, i.e., the null point, is assumed to be identical to the surface temperature history. Then, the temperature at the null point can be inserted into a one-dimensional inverse heat conduction problem for a semi-infinite solid to determine the heat flux at the surface. The theoretical assumption of one-dimensional and linear heat conduction is strengthened by an appropriate sensor design (see Fig. 2). Because of the high enthalpy flow condition, the essentially uncooled sensors have to be passed very quickly across the flow diameter. The sensors in the current configuration are moved with a velocity of 1 m/s across the flow. Considering the plasma flow diameter of about 30 mm, one heat flux measurement is performed in 0.03 s, which is about half the time the sensor is supposed to be used [1,4]. However, the recorded temperature profile allows to deduce the heat flux along the measured direction, i.e., perpendicular to the flow axis, which is the radial profile.

For the temperature measurement itself, there are historically three different approaches: coaxial surface thermocouples, thin-film resistance thermometers, and null-point calorimeters. As mentioned, the fundamental assumption in the heat flux estimation using such devices is that of linear one-dimensional heat conduction. If a homogeneous temperature between the probe surface and the measurement location during the experiment can be assumed, the thin-film theory is applied and the heat diffusion problem can be solved analytically [5]. In contrast, the thick-film theory means that it is assumed that the temperature at the opposite end of the surface which is exposed to the heat flux rests constant throughout the experiment, which corresponds to semi-infinite behavior and leads also to an analytical solution. Usually, the thin-film theory is applied to resistance thermometers and the thick-film theory to surface thermocouples and null-point calorimeters. To characterize the plasma flow, the radial profile of heat flux has to be measured, which is only applicable to sensors according to the thick-film theory [4]. However, as will be shown later, the especially short measurement times lead to the conclusion that the one-dimensional conditions are no longer valid. Moreover, the thermocouple's junction never reaches a homogeneous temperature level during exposure time, which means that the measured signal, that is a voltage drop, cannot be related to the junction temperature using the thermoelectric calibration as it is proposed up to now. Hence, this well-known measurement technique has to be further investigated to adapt it to

Received 27 March 2007; revision received 8 October 2007; accepted for publication 22 October 2007.

*Research Engineer, Laboratoire TREFLE, Esplanade des arts et métiers, 33405 Talence; stefan.loehle@dlr.de. Member AIAA.
†Professor, Laboratoire TREFLE.
‡Research Engineer, Avenue du Général Niox.
§Research Engineer, Route des Gargails.

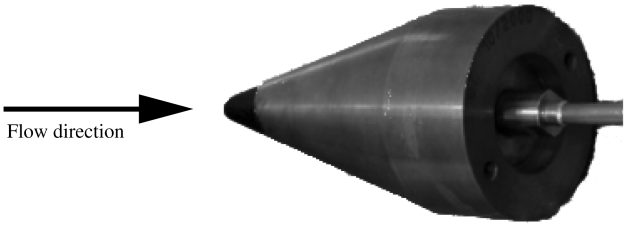

Fig. 1 Photography of null-point calorimeter (AQ28).

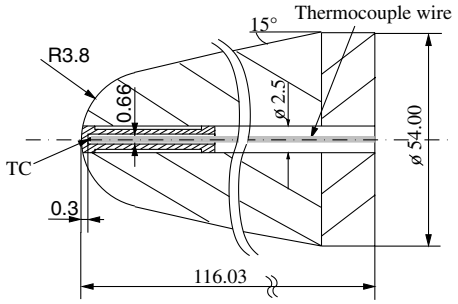

Fig. 2 Sectional view and dimensions (in millimeters) of the probe.

currently investigated high enthalpy as well as high-pressure environments, where heat fluxes in the range of several tens of MW/m^2 at pressures of several tens of bars are expected. In a first measurement campaign at the Laboratoire National de Métrologie et d'Essais (LNE), the response behavior with respect to short measurement times has been investigated [6].

The present paper deals with a reconsideration of the null-point calorimeter using modern data analysis and a new piloted high-power laser source for calibration. It will be shown that this approach permits a significant improvement of the rather classical heat flux measurement technique for high heat flux applications.

The following section introduces in the experimental aspects of high heat flux estimation followed by a description of the used sensor and calibration setup. The theoretical approach, as well as a description and interpretation of the experimental results, follow.

II. Heat Flux Sensor

For the aforementioned measurement purpose, a commercially available heat flux sensor, as shown in 1, is used. In fact, two sensors of the same design have been investigated. A null-point calorimeter consists of a rather big copper part, with conical flanks and a spherical tip (see Fig. 2). The tip itself is originally manufactured as a separate part and the heat flux sensor is revised after the tip is inserted to finalize the spherical form [7]. The advantage of such a two-piece design is that the positioning of the thermocouple, which is an essential concern when using classical data treatment, can be carried out properly before it is inserted in the bigger part. Furthermore, an additional air gap shall strengthen the assumption of a one-dimensional behavior, i.e., avoid radial heat conduction. To investigate the crucial influences of measurement time, thermocouple position, and radial heat conduction, the sensor has been investigated theoretically. Figure 3 shows the finite element model that has been used. The commercially available computer program Comsol/FemLab has been used. Although the whole sensor has been modeled, only the critical part at the tip is shown in the figure, in which the used thermophysical properties are marked, too. As can be seen in the figure, a very detailed model, including the thermocouple wire, isolation, and fitting adhesive, has been drawn. The material constants are taken from databases [8]. The mesh generated by Comsol/Femlab with 6986 elements is checked by the internal quality parameters. Usually, a quality of >30% is sufficient to guarantee that the mesh quality does not affect the quality of the solution [9]. In the present case, the mesh quality has been >70%.

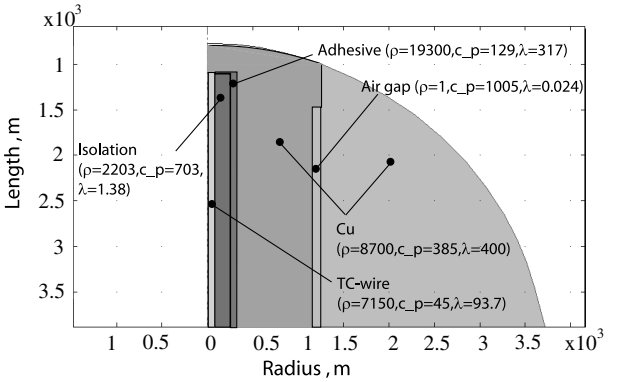

Fig. 3 Detailed finite element model of the sensor tip [ρ in kg/m^3, c_p in $J/(kg \cdot K)$, λ in $W/(m \cdot K)$].

The principle equation for one-dimensional heat conduction in every part of the system is given by the heat equation, which is

$$\frac{\partial T}{\partial t} = \frac{\lambda_i}{\rho_i c_{p_i}} \frac{\partial^2 T}{\partial x^2} \tag{1}$$

In this relation, ρ_i denotes the density, c_{p_i} is the specific heat, and λ_i the thermal conductivity for each material i for each part of the heat flux sensor [5]. The boundary conditions are the heat flux that is imposed on the spherical tip (see Fig. 1) and a constant temperature on the opposite end of the cone. Because of the usually supersonic plasma flow, it is assumed that mainly the spherical tip is affected by the hot plasma.

Using this model, the effect of correct positioning of the thermocouple can be investigated. As can be seen from Eq. (1), the position x of the thermocouple is one of the decisive variables when assuming one-dimensional heat flux. Figure 4 shows that an error in the estimation of the position of only 0.05 mm corresponds to an error in temperature of 5% with respect to the temperature at the nominal position. Although this error is not huge, its influence on the estimated heat flux is significant. The deviation of 5% in temperature leads to a difference in heat flux of about 20% with respect to the nominal position. As will be shown within the calibration section, a significant improvement of the heat flux measurement is already achieved due to the fact that a method is used to calibrate the sensor in which the exact positioning does not have to be known.

A second crucial item of this sensor concerns the short measurement times. Figure 5 shows the response time of a thermocouple type K. For this calculation, a spherical junction form has been assumed and the material constants of nickel have been used [10]. Although this calculation is, due to the assumed geometrical

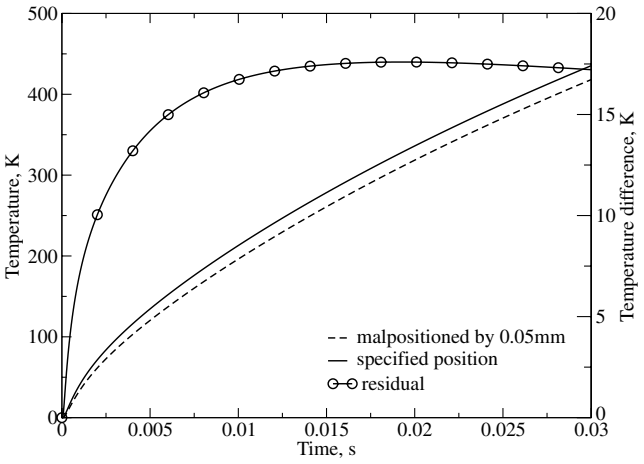

Fig. 4 Influence of different positions of the thermocouple on the measured temperature.

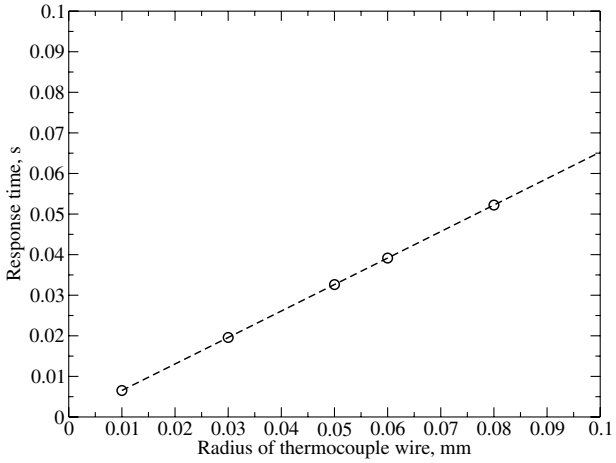

Fig. 5 Thermocouple junction inertia.

simplicity, only a rough estimation, it can nevertheless be seen that the thermocouple in use with a diameter of 0.16 mm never reaches a homogeneous temperature level during the measurement time of 0.03 s. Thus, the measured signal (in volts) can not be transferred to a temperature value (in Kelvin). As will be shown, the applied calibration technique does not depend on this relation, a relative temperature signal is sufficient, and the thermocouple inertia is accounted for.

III. Calibration

The main idea in the calibration stage is to heat the null-point calorimeter using a laser on the same area as that concerned during measurement in the plasma jet and to calibrate the sensor taking into account its time response. Because the applied radiative heat flux on the surface is known, the two quantities, heat flux and temperature, can be related. This procedure is known in the field of automation and control as the system identification process. The system identification and the calculated impulse response of the heat flux sensor are described in detail in [6]. The main steps are nevertheless described in the following section.

It can be shown that the temperature in monovariable thermal systems can be expressed according to the temperature at each point of the domain in the form

$$\sum_{n=M_0}^{M} \alpha_n D^{n/2} V_T(t) = \sum_{n=L_0}^{L} \beta_n D^{n/2} \phi(t) \quad \text{with} \quad \alpha_{M_0} = 1 \qquad (2)$$

The operator D stands for the differentiation of the order indicated by the superscript [11], V_T is the thermocouple signal, and ϕ the heat flux. Equation (2) is known as the noninteger model. In one-dimensional heat diffusion configurations, the parameters α_n and β_n can be directly expressed by the thermophysical properties of the system. However, in more complex systems, as the one studied here, this link cannot be analytically found. The form of the model, though, remains exact when $M \to \infty$ and $L \to \infty$. Nevertheless, very good accuracy is found when considering small values of M and L. Noninteger derivatives are representative of the semi-infinite behavior of the system. If a calibration measurement is performed, such that a known heat flux is imposed on the sensor and the resulting temperature increase is measured, the unknown coefficients α_n and β_n can be identified, whereas the fractional derivatives have to be calculated. In the present case, the fractional derivatives are calculated following the method of Grünwald [12]. The following calculation of the impulse response leads to a fully identified system including all geometrical, as well as all temporal, effects, the latter of which depends on the measured time scale. The experimental realization of this method is described in the following section.

IV. Experimental Setup

Figure 6 shows a schematic of the experimental setup for the calibration measurements. A continuous-wave diode laser system (DILAS DFx20-980) that emits at a wavelength of 980 nm is operated with a function generator (Agilent 33120A) to generate heat flux impulses of different lengths. The spatial intensity distribution, as well as the beam diameter, have been measured using laser analysis equipment (WinCamD) at the measurement location (see Fig. 7), although the intensity distribution over the laser beam area is, due to the use of an optical fiber, very homogeneous. Because the calibration depends strongly on the heated area, the beam diameter has to be measured very accurately. The optical head of the diode laser has a focal length of 100 mm and a focusing lens with a diameter of 40 mm. The distance at which a beam diameter of 3.8 mm is attained has been calculated from geometrical relations to be 120 mm. The measured beam diameter at this distance, using the laser beam analyzer, gives a beam diameter of 3.8 ± 0.5 mm. Because of the mentioned optical fiber, the beam profile is easily determined, because the border occurs as a discrete step. The laser impulses are logged using a photodiode next to the heat flux sensor. All measured data, i.e., the amplified thermocouple voltage and the diode signal, are recorded using a fast oscilloscope (LeCroy Waverunner LT364) and saved on a personal computer for data treatment. The approach described in Sec. III is applied to the measured data using MATLAB.

In the present case, it is assumed that the heat flux sensor is mostly affected at the spherical tip, which has been numerically proven by calculation of the heat transfer (see Fig. 8) [13]. Nevertheless, Fig. 8 shows that the conical part is affected and certainly has an influence on the measured heat flux, but comparing the very high heat flux at the tip with the low heat flux to the conical flanks, it is assumed that this influence is negligible. Hence, the calibration has to be performed on an area of the diameter of the spherical tip which is 7.6 mm. On the other hand, the laser cannot reach the same heat flux density as in the plasma jet (about 60 $\mathrm{MW/m^2}$). However, it has been shown by previous measurements that the system behaves linear with

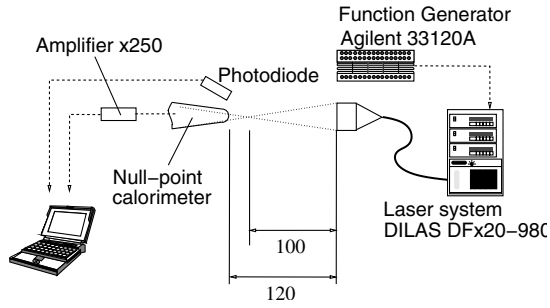

Fig. 6 Schematic of the experimental setup.

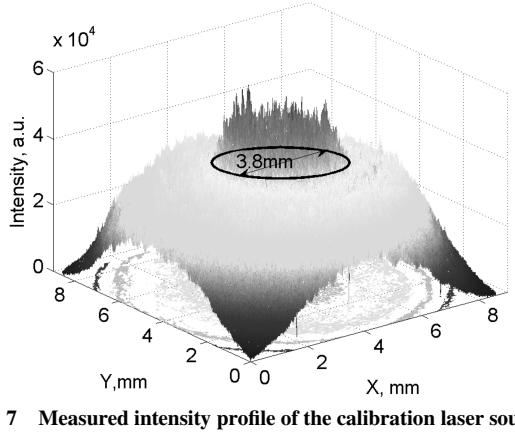

Fig. 7 Measured intensity profile of the calibration laser source.

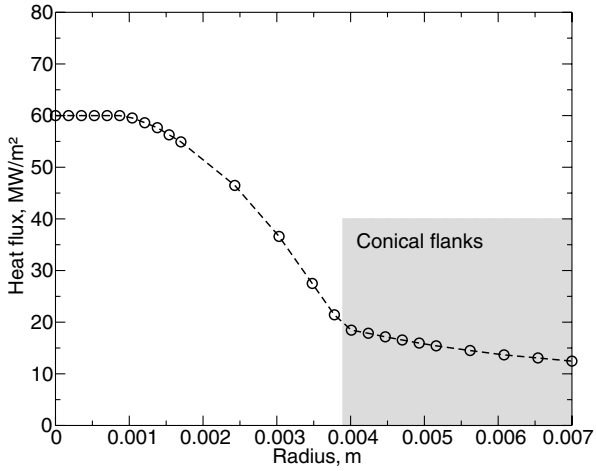

Fig. 8 Numerical result of the heat transfer to the tip of the null-point calorimeter.

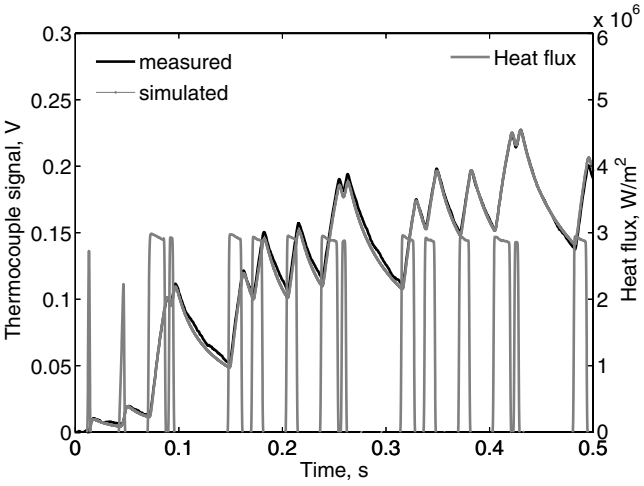

Fig. 10 Calibration measurement for sensor AQ28.

respect to the heat flux, i.e., doubling the incoming heat flux results in twice the thermocouple signal under the previously explained assumptions [6]. Thus, a lower calibration heat flux is sufficient, as long as the time behavior can be accounted for. To get enough thermocouple data within the very short measurement times (about 0.05 s), laser power on the order of 150 W is needed.

Finally, to account for the emissivity of the sensor surface, emissivity measurements have been performed at Commissariat à l'Energie Atomique (CEA). For the oxidation state of the surface as it appears after plasma wind-tunnel testing, an emissivity of $\epsilon = 0.7$ has been measured [14].

V. Results

A. Calibration Results

To resolve the temporal behavior of the sensor, different time intervals of heat flux during calibration have to be accounted for. A pseudorandom signal sequence is computed for each calibration. This signal sequence is used for the laser gating using the function generator (see Sec. IV). Figures 9 and 10 show the calibration measurement of each sensor. As can be seen, different time intervals of heating have been conducted while the maximum calibration heat flux is about 4 $\mathrm{MW/m^2}$. The smallest time interval is 0.002 s. It has to be pointed out that the measured thermocouple signal is treated as a raw data in volts. As explained before, this is recommended to account for the thermocouple inertia.

The agreement between the identified temperature sequence and the measured one is sufficiently well. The identified systems are

$$(1 - 0.053 \pm 6.536 \cdot 10^{-10} D^{0.5} + 0.0012 \pm 2.55 \cdot 10^{-11} D - 1.169 \cdot 10^{-5} \pm 3.83 \cdot 10^{-13} D^{1.5} + 5.045 \cdot 10^{-8} \pm 2.423 \cdot 10^{-15} D^2) V_T(t) = (-9.335 \cdot 10^5 \pm 0.529 + 3.0631 \cdot 10^6 \pm 0.121 D^{0.5} + 2055.8 \pm 0.004 D^1) \phi(t) \quad (3)$$

for the first (AQ24) and

$$(1 - 0.07685 \pm 5.0806 \cdot 10^{-9} D^{0.5} + 0.0024 \pm 3.4292 \cdot 10^{-10} D - 3.6809 \cdot 10^{-5} \pm 8.1123 \cdot 10^{-12} D^{1.5} + 2.4964 \cdot 10^{-7} \pm 7.8708 \cdot 10^{-14} D^2) V_T(t) = (1.786 \cdot 10^6 \pm 0.21152 + 2.0812 \cdot 10^6 \pm 0.1089 D^{0.5} + 3.7382 \cdot 10^4 \pm 0.01921 D) \phi(t) \quad (4)$$

for the second calorimeter (AQ28). Using these model data, the impulse response is calculated [6]. Figure 11 shows the impulse responses for both sensors. The two sensors behave obviously not identical, i.e., they are not manufactured identically. Because the deviation in the system identification process is very small [see Eqs. (3) and (4)], this influence is negligible. The calibration setup has not been changed to investigate the two sensors, hence its accuracy is similar. So, the reasons for the difference are actually due

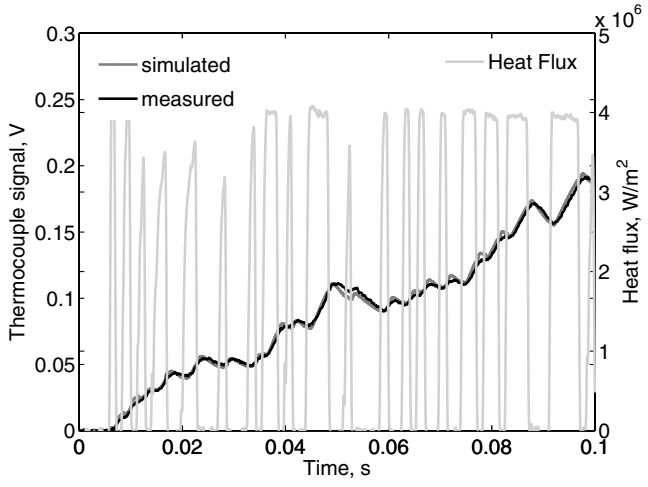

Fig. 9 Calibration measurement for sensor AQ24.

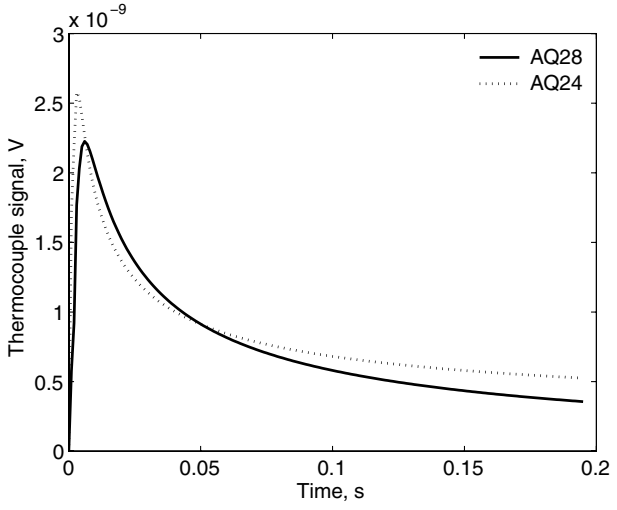

Fig. 11 Impulse response for both sensors.

to real manufacturing and material differences between the two sensors as, for example, the aforementioned position of the thermocouple or the used copper material.

B. Plasma Wind-Tunnel Results

Both null-point calorimeters have been used in the high-pressure, high-enthalpy facility at European Aeronautic Defence and Space Company–Space Transportation (EADS-ST), called JP200 [15]. It consists of four crosswise arranged Huels-type arcjet generators. The maximum electric input power is 20 MW resulting in flow enthalpies of about 20 MJ/kg at total pressures of about 60 bar and heat fluxes of about 60 MW/m^2. As mentioned in the Introduction, the calorimeter passes the jet radially at high speed while the thermocouple data is stored. Figure 12 shows the recorded signals. Only one heat flux probe can be mounted for each test and hence two tests were performed at two different plasma conditions. From the thermocouple data in Fig. 12, it is obvious that with the sensor AQ24, considerably higher temperature signals have been measured.

Applying the new approach, a symmetrical profile is measured with both sensors, as it is expected from freejet theory [16]. Additionally, the classical approach using the concept of null-point calorimetry is plotted in Fig. 13 and for each curve, one exemplary error bar is added. The measured heat flux using this one-dimensional approach is slightly lower than the heat flux estimated using the new calibration measurements. However, it has to be noted that for the classical approach, the thermophysical properties of the copper material are needed, whereas the system identification approach does not need any of these values.

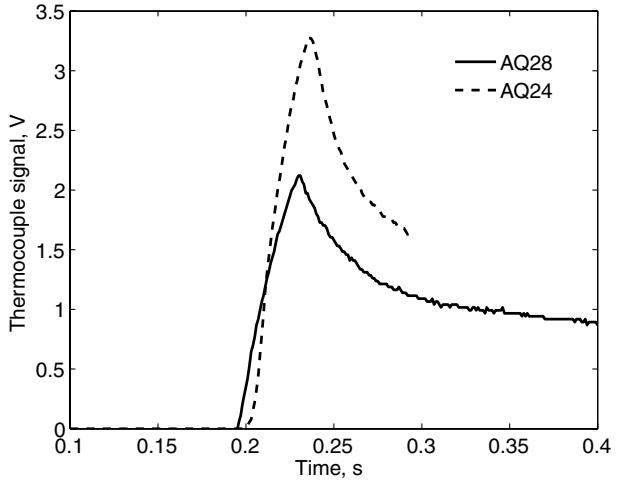

Fig. 12 Thermocouple signal for both sensors during two different plasma wind-tunnel tests.

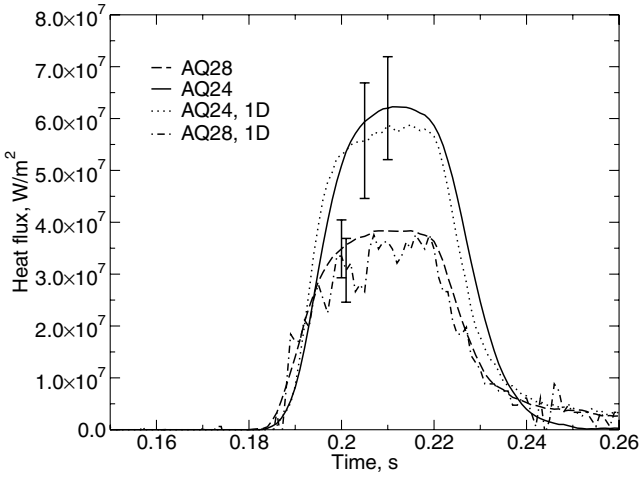

Fig. 13 Measured heat flux at two generator conditions using two different calorimeters.

VI. Measurement Accuracy

The most important source of error is within the calibration step. The laser output power has an accuracy of 10% and the measurement of the laser beam area is quite sensitive [17]. The radius of the measurement area has, on the one hand, been calculated from geometrical optics and, on the other hand by using the laser beam analyzer as mentioned before. Both methods lead to an accuracy of 3.8 ± 0.1 mm, which corresponds to about 3%. In general, measurement errors are calculated using

$$\frac{\Delta f}{f} = \sum_i \left|\frac{\partial f}{\partial x_i}\right| \frac{\Delta x_i}{f} \tag{5}$$

where f stands for the measured function depending on different variables x_i. In the present case, the depending variables are the radius of the measurement area r and the laser energy E. The function f is thus $f = E/(\pi r^2)$. Hence, Eq. (5) becomes

$$\frac{\Delta f}{f} = \left|\frac{1}{\pi r^2}\right| \frac{0.1 \cdot E}{f} + \left|\frac{-2E}{r^3}\right| \frac{2.6 \cdot r}{f} \tag{6}$$

With the assigned accuracy levels, the heat flux can be calculated with an overall accuracy of 16%, which is better than the 20% accuracy estimated for the conventional data analysis [18].

VII. Conclusions

A new method to estimate the heat flux using classical null-point calorimeters is presented. From a finite element analysis, it can be concluded that the one-dimensional, semi-infinite heat conduction approach is not applicable for the very short measurement times in EADS-ST plasma wind tunnels. The main reasons are the high thermocouple inertia with respect to the measurement time and radial heat fluxes.

The new calibration method based on measurements using a high-power laser radiation source, together with system identification using a direct noninteger model, shows that the previously measured asymmetries in the radial heat flux profiles are due to the one-dimensional, semi-infinite approach. Furthermore, the calibration is applied to the raw thermocouple signal, and hence the inertia of the thermocouple for the short measurement times of interest is taken into account. The measured heat flux value on the centerline of the jet is estimated to be slightly higher than from the classical approach. This is probably an effect of the different materials used, and hence the different material properties inserted in the model using the approach of null-point calorimetry.

Acknowledgment

The authors would like to thank Jean-Christophe Batsale for his invaluable contribution to this publication.

References

[1] Kennedy, W., Rindal, R., and Powers, C., "Heat Flux Measurement Using Swept Null Point Calorimetry," *Journal of Spacecraft and Rockets*, Vol. 9, No. 9, 1972, pp. 668–675.

[2] Kidd, C., "High Heat Flux Measurements and Experimental Calibration/Characterizations," NASA TR CP-3161, 1990.

[3] Kidd, C., "Recent Developments in High Heat Flux Measurement Techniques at the AEDC," *Proceedings of the 36th International Instrumentation Symposium*, Instrument Society of America, Research Triangle Park, NC, May 1990, pp. 477–492.

[4] "Standard Test Method for Measuring Extreme Heat-Transfer Rates from High-Energy Environments Using a Transient, Null-Point Calorimeter," American Society for Testing and Materials, TR E598-96, 2002.

[5] Carslaw, H., and Jaeger, J., *Conduction of Heat in Solids*, Oxford Univ. Press, Oxford, England, U.K., 1959.

[6] Löhle, S., Battaglia, J.-L., Batsale, J.-C., Enouf, O., Dubard, J., and

Filtz, R.-R., "Characterization of a Heat Flux Sensor Using Short Pulse Laser Calibration," *Review of Scientific Instruments*, Vol. 78, No. 5, May 2007.
doi:10.1063/1.2736388

[7] Operating Manual: Null-Point Heat Flux Processor, Acurex Users Manual UM-84-10/ATD, Acurex Corp., Mountain View, CA, 1984.

[8] "NIST Chemistry WebBook," National Inst. of Standards and Technology, 2006, www.nist.gov.

[9] Femlab 3.0 User's Guide, Comsol AB, Stockholm, 2004.

[10] Traité de thermométrie par thermocouple et résistance, Société TC Direct, Mönchengladbach, Germany, 2001.

[11] Battaglia, J.-L., *Méthodes d'Identification de Modèles à Dérivées d'ordre non ontier et de réduction modale*, Habilitation, Université Bordeaux 1, Lab. Interetablissement TREFLE, 2002.

[12] Battaglia, J.-L., Cois, O., Puigsegur, L., and Oustaloup, A., "Solving an Inverse Heat Conduction Problem Using a Non-Integer Identified Model," *International Journal of Heat and Mass Transfer*, Vol. 44, No. 14, 2001, pp. 2671–2680.
doi:10.1016/S0017-9310(00)00310-0

[13] Jullien, P., and Foltyn, M., "Etude Thermique du Fluxmètre Point nul," European Aeronautic Defence and Space Transportation, TR TE31-045313/04, 2004.

[14] Cerisier, M., "Campagne C108: Caractérisation Optique du Cuivre ARA," Commissariat à l'Energie Atomique, Internal Rept. CEA/CESTA, TR DO 577, 2006.

[15] Boursereau, F., Donnart, P., Bouffet, S., Astier, J.-C., Jullien, P., and Foltyn, M., "Theoretical and Experimental Investigations on a New Test Configuration on Arc Heater," *4th International Symposium on Atmospheric Reentry Vehicles and Systems*, Assoc. Aeronautique et Astronautique de France (3AF), Paris, 2005.

[16] Abramovich, G., *Theory of Turbulent Jets*, MIT Press, Cambridge, MA, 1963.

[17] Manuel de l'utilisateur DILAS Laser à Diodes Série DFX, DILAS, Mainz, Germany, 2006.

[18] Kennedy, W., Rindal, R., and Powers, C., "Heat Flux Measurement Using Swept Null Point Calorimetry," *6th AIAA Thermophysics Conference*, AIAA, 1971.

J. Olejniczak
Associate Editor